Desalination and Water Treatment
www.deswater.com

doi: 10.5004/dwt.2019.23674

145 (2019) 120–133
March

Evaluation of a polymaleic-based scale inhibitor (HPMA-AEO-9) against calcium carbonate scale

Chen-Guo Zhu[a], Wei-Dong Zhao[a], Hong-Bin Liu[a], Yao Che[a], Liang-Bi Wang[b,c], Qiao-Ling Zhang[a], Liang-Chen Wang[a,c,*]

[a]*School of Chemical Engineering, Lanzhou Jiaotong University, 88 West Anning Rd., Lanzhou 730070, China, email: 739088624@qq.com (C.-G. Zhu), 1165963092@qq.com (W.-D. Zhao), hongbinliu163@163.com (H.-B. Liu), 273851077@qq.com (Y. Che), 739931717@qq.com (Q.-L. Zhang), Tel. +86-931-4956556, Fax +86-931-4956556, email: lcwang1967@163.com (L.-C. Wang)*

[b]*Department of Mechanical Engineering, Lanzhou Jiaotong University, 88 West Anning Rd., Lanzhou 730070, China, email: lbwang@mail.lzjtu.cn (L.-B. Wang)*

[c]*Key Laboratory of Railway Vehicle Thermal Engineering (Lanzhou Jiaotong University), Ministry of Education, China*

Received 25 April 2018; Accepted 25 December 2018

ABSTRACT

Hydrolyzed polymaleic anhydride (HPMA) is widely used as a scale inhibitor, but it is easy to form insoluble gel with alkaline earth ions. To overcome this shortcoming, a fatty alcohol ethoxylate (AEO-9) is introduced into HPMA to obtain a maleic acid-based copolymer HPMA-AEO-9. HPMA-AEO-9 is characterized by FT-IR, ^{1}H NMR and GPC. The effects of HPMA-AEO-9 on $CaCO_3$ scale are studied in several aspects (such as dose, Ca^{2+} concentration, temperature, inhibition time, pH, and the relative supersaturation of $CaCO_3$ solution) by static experiments. The effect of HPMA-AEO-9 on the scaling process is studied under dynamic conditions. The impact of HPMA-AEO-9 on morphologies of $CaCO_3$ is investigated using SEM and XRD. The results show that the presence of AEO-9 group can significantly improve the resistance of HPMA-AEO-9 to high alkalinity, high hardness and high temperature. Compared with additive of HPMA, the presence of HPMA-AEO-9 can obviously inhibit the nucleation rate at the induction region, accelerate the growth of nuclei at the rapid growth region, and reduce the scaling rate at the stable growth region; HPMA-AEO-9 changes calcium carbonate crystal from stable calcite to unstable aragonite and vaterite. HPMA-AEO-9 is a threshold inhibitor with excellent performance in inhibiting $CaCO_3$ scale.

Keywords: Circulation cooling water; Calcium carbonate scale; Maleic acid; Antiscalant; Fatty alcohol polyoxyethylene ether (AEO)

1. Introduction

The deposit of scale can reduce flow rate, increase energy consumption remarkably, and endanger the normal operation of the equipment [1,2]. In order to reduce the losses caused by mineral scaling, the most efficient and economic method is to deliver scale and corrosion inhibitor into circulation cooling water system [3].

Polymer antiscalants are referred to a class of agents that can disperse, prevent or interfere with the insoluble inorganic salts in water to deposit as scaling on the heat transfer surface [4,5]. In recent years, with the strengthening of environmental protection consciousness, phosphorus class scale inhibitors are strictly restricted because it can cause water eutrophication; hence green environmentally friendly polymer inhibitors have attracted more research attention [6,7]. The performance of polymer inhibitors is highly dependent on their polymer structure, functional groups and molecular weight. For instance, polyaspartic acid (PASP) is a type of green antiscalant with a hydrophilic polyamino acid backbone linked by different side chains (–CH_2COO^- and –COO^- groups) [8]. The hydrophilic polyamino acid back-

*Corresponding author.

bone enhances the solubility of PASP in water. The different carboxyl acid side-chains in the molecule have a certain stabilizing effect on the alkali metal ions in water, and the effects of PASP on $CaSO_4$ and $CaCO_3$ scales largely depend upon its mean molecular weight, molecular weight distribution, degree of side-chaining and purity [9,10]. Antiscalants based on polycarboxylic acid such as poly(acrylic acid) [11] and poly(maleic acid) [12–14], containing a large number of carboxyl groups in their molecular, are more environmentally acceptable due to their intrinsic biocompatibility, biodegradability, and non-toxicity. However, owing to the weak acidity of the carboxyl group, these polymers can form insoluble gel with alkaline earth metal ions in water [15,16], limiting their inhibition performance remarkably. Advances in the chemical modification of these polymers are mainly based on overcoming the limitations of physicochemical property. For example, an alternating copolymer of acrylic acid (AA)-allyloxy poly (ethylene glycol) polyglycerol carboxylate (APEG-PG-COOH) displays a superior ability over other inhibitors (such as PESA, HEDP, PAA and PBTC) in controlling inorganic minerals scales, owing to the presence of a number of ethylene glycol and carboxyl groups in its molecular [17]. A series of well-characterized-PAA, obtained through introduced some hydrophobicity groups into PAA molecular, are found that both end groups and molar masses play an important role in inhibiting decomposition of HCO_3^- which is usually related to the concentration of alkaline-earth metal ions in circulation cooling water [18]. Generally, the higher the HCO_3^- concentration, the higher the concentration of alkaline earth metal ions dissolved in water. A double hydrophilic block copolymer, prepared from allylpolyethoxy carboxylate (APEC) and acrylic acid (AA), exhibits excellent ability to prevent $CaCO_3$ and $CaSO_4$ scale [19], which is ascribed to interactions between $CaCO_3$ crystal and carboxylic ion, ethylene oxide (EO) group and Ca^{2+} ions. A novel acrylic acid-allylpolyethoxy carboxylate copolymer (AL15) has excellent performance in the corrosion inhibition and the scale inhibition [20], owing to the presence of different length side chaining such as polyether succinate and carboxylic ion on its backbone. Betz Company (U.S.A) has developed an acrylic-allyloxy polyethoxy sulfate copolymer (AA-APES) with different length of the side chaining (carboxyl and sulfonic acid groups as well as ethoxy group) on its backbone [21]. This modification greatly improves the inhibition performance against calcium phosphate scale but fails to prevent $CaCO_3$ scale effectively. It is clear that the excellent inhibitory properties of polymer inhibitors are mainly determined by the following characteristics: the polymer with a good solubility in water, at least two or more functional groups with different chain lengths connected to the polymer backbone, certain average molecular weight and molecular weight distribution [22].

Fatty alcohol polyoxyethylene ether (AEO-9), being as a non-toxic and phosphorus-free surfactant, has good calcium tolerance due to the presence of EO groups in its molecular structure [23]. The presence of EO groups could enhance the solubility of the polymer inhibitors and the ability to disperse inorganic minerals scales [17–20]. The introduction of EO groups into polymaleic anhydride (HPMA) molecular might change the solubility of HPMA and enhance its effects on Ca^{2+}, Mg^{2+} and Ba^{2+} in the bulk solution.

In this paper, HPMA-AEO-9 is prepared from maleic anhydride, fatty alcohol ethoxylates (AEO-9), ammonium ferric sulfate and hydrogen peroxide. The primary objective of this work is to determine the effects of AEO-9 group on the scale inhibition performance of HPMA-AEO-9 against $CaCO_3$ scale. The influences of dosing and operation conditions on the performance of HPMA-AEO-9 against $CaCO_3$ scale are studied by static tests. The effect of HPMA-AEO-9 on the scaling process of the tube wall is investigated under dynamic conditions. The influence of HPMA-AEO-9 on the relative supersaturation of $CaCO_3$ solution is also investigated using conductivity method, and the impact of HPMA-AEO-9 on morphologies of $CaCO_3$ is studied using SEM and XRD.

2. Material and methods

2.1. Reagents and instruments

Ethylene diamine tetraacetic acid (EDTA), calcium nitrate, sodium bicarbonate, sodium carbonate, sodium hydroxide, ammonium ferric sulfate, maleic anhydride (MA), sodium sulfate and sodium phosphate are analytical reagents and purchased from Tianjin No. 6 Chemical Reagent Factory (Tianjin, China). Hydrogen peroxide (30%) is purchased from Tianjin Benchmark Chemical Reagent Co. Ltd. (Tianjin, China). Fatty alcohol ethoxylates (AEO-9), as molecule type $C_{12}H_{25}(CH_2CH_2O)_9OH$, is technical grade and supplied by Haian Chemical Factory (Jiangsu, China). Hydrolysis polymaleic acid (HPMA, 480 M_W), polyacrylic acid (PAA, 3000 M_W) and hydroxyethylidene diphosphonic acid (HEDP, 206 M_W) are technical grade and purchased from Shandong TaiHe Water Treatment Technologies Co., Ltd. (Shandong province, China). All the above chemicals are used as received from the manufacturers.

Instruments used in this research included Quanta 200 (USA) scanning electronic microscope (SEM), FA2004B electronic balance, Gel permeation chromatographic (GPC, Agilent 1100), Nexus670SX for recorded FT-IR spectra, and AVANCE III HD 500 (Switzerland) Superconducting nuclear magnetic resonance spectrometer.

2.2. Synthesis of HPMA-AEO-9

2.2.1 General monomer synthesis

As illustrated in Eq. (1), MA-AEO-9 is prepared from AEO-9 and maleic anhydride (MA). 29.0 g AEO-9 and 5.4 g MA (the molar ratio of MA: AEO-9 is 1:1.1) are added in a 100 mL round bottom flask and stirred with a magnetic stirrer, then the flask is placed in an oil bath and maintained at 70 °C for 4h, and finally MA-AEO-9 (a light-yellow liquid) is obtained.

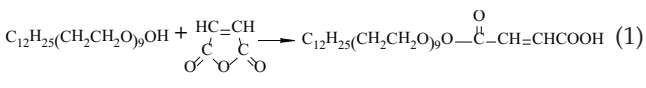

$$C_{12}H_{25}(CH_2CH_2O)_9OH + \underset{\underset{O}{\overset{\|}{C}}\quad\underset{O}{\overset{\|}{C}}}{HC=CH} \longrightarrow C_{12}H_{25}(CH_2CH_2O)_9O\text{—}\overset{O}{\overset{\|}{C}}\text{–}CH=CHCOOH \quad (1)$$

2.2.2. Synthesis of HPMA-AEO-9 copolymer

As shown in Eq. (2), HPMA-AEO-9 is prepared by the way of free radical copolymerization. 5.9 g MA and 6.9 g MA-AEO-9 (the mole ratio of MA to MA-AEO-9 is 6:1) as well as 0.11 g ammonium ferric sulfate (0.04 mol% of the total monomer) are dissolved in 24 mL distilled water in

a 100 mL three necked round-bottomed flask equipped a thermometer and a dropping funnel and a water-cooled glass condenser. The reaction is then heated to 90°C and 5 g (30%) hydrogen peroxide (7.5 mol% of the total monomer) in 11 mL distilled water is dropped wise to the mixture solution within 1.5 h, followed by further conversion at 95°C for 2 h. Ultimately, a light purple HPMA-AEO-9 solution is obtained with the solid content of 25 wt% [24]. The resulting solution is dried under vacuum, washed with ethanol, filtered and dried in vacuum to give HPMA-AEO-9.

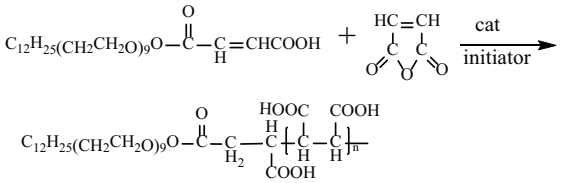

(2)

2.3. Evaluation of antiscalant behavior

2.3.1. Inhibition performance of antiscalants against $CaCO_3$ scale under the static conditions

The inhibition performance of HPMA-AEO-9 against $CaCO_3$ scale is investigated according to the China National Standard (GB/T16632-2008) under static conditions [25]. The artificial water specimens, $\rho(Ca^{2+}) = \rho(HCO_3^-) = 250$ mg/L (as $CaCO_3$) with different dosage of antiscalants and pH of 9.0 (adjusted with borax), are maintained at 80°C for 10 h in water bath, then the remaining Ca^{2+} is titrated by EDTA standard solution and compared with the blank test [26]. The inhibition efficiency, %I, is defined as:

$$Percent\ Inhibition\ (\%I) = \frac{V_2 - V_1}{V_0 - V_1} \times 100 \quad (3)$$

where V_0 and V_1 are the volume of EDTA without inhibitor at the starting and after incubation, respectively, V_2 is the volume of EDTA with inhibitor after incubation. The maximum uncertainty in %I value is determined within ±2%.

2.3.2. Inhibition performance of antiscalants against $CaCO_3$ scale by conductivity method

The experiment of conductivity method is used to evaluate the performance of HPMA-AEO-9 to inhibit calcium carbonate precipitation in aqueous solution. The test solutions for crystal growth experiments are prepared by dropwise add equal volumes of Na_2CO_3 (0.1 M) to $CaCl_2$ solutions (0.1 M) (containing a variable amount of the inhibitor) at 36±0.1°C as method reported in the literature [27]. With the presence of inhibitor, the relative supersaturation of the $CaCO_3$ solution, S_r, is calculated from:

$$S_r = S_p / S_0 \quad (4)$$

$$S = [Ca^{2+}] \times [CO_3^{2-}] / K_{SP}(T) \quad (5)$$

where S_p is the supersaturation of $CaCO_3$ in the presence of inhibitor, S_0 is the supersaturation of $CaCO_3$ in the absence of inhibitor, and $K_{SP}(T)$ is the solubility product of $CaCO_3$ at 36°C.

2.3.3. Inhibition performance of antiscalants against $CaCO_3$ scale under the dynamic conditions

To evaluate the scaling performance of HPMA-AEO-9 against $CaCO_3$ scale under the working conditions, experiments are conducted by a simulation cooling water circulation system which is reported in our previous study [28].

The test solution, 360 mg/L HCO_3^- and 240 mg/L Ca^{2+} and dosage of the inhibitor of 8 mg/L, is prepared with deionized water. In each run, the test solution is pumped through the test tube of heat exchanger by magnetic pump, and then returned to the solution tank through the circulation system.

The experimental conditions are listed in Table 1, and run times are included 6, 12, 18, 24, 30, 40, 50, 60 and 70 h. After each run time, the test tube is pulled out the double

Table 1
The operating conditions of the double pipe heat exchanger

Parameter	HPMA	HPMA-AEO-9
The tube of the double pipe heat exchanger:		
Flow	The test solution	
The test tube (AISI 316L)	ø8×1±0.05 mm	
Flow velocity [L/h]	20	20
Reynolds number (*Re*)	1800	1800
$\rho(Ca^{2+})$ [mg/L]	240	240
$\rho(HCO_3^-)$ [mg/L]	360	360
Dosage of inhibitor [mg/L]	8	8
Inlet temperature [°C]	50±1	50±1
Outlet temperature [°C]	60±1	60±1
The shell of the double pipe heat exchanger:		
Flow	Hot water	
Reynolds number (*Re*)	6000	6000
Inlet temperature [°C]	75±1	75±1
Outlet temperature [°C]	73±1	73±1

pipe heat exchanger, and then placed in an oven at 50°C for 24 h, and finally weighed using an analytical balance (± 0.0001 g). The deposition of $CaCO_3$ scale on the test tube wall can be obtained by comparison with the mass of the test tube before and after each run. The mean deposition on the test tube wall, w, is defined as:

$$w = \frac{\Delta w}{A} \tag{6}$$

where Δw is the mass increment of $CaCO_3$ scale deposited on the surface of the test tube, A is internal surface area of the test tube.

When the run time reaches at 12, 24 and 70 h, the deposition of $CaCO_3$ scale is sampled (using a sampling bolt ø4×3 mm) at the midpoint of the test tube and then analyzed using a high-resolution scanning electron microscope (SEM). The maximum uncertainty in the mean deposit on the test tube wall is determined to be within ± 20% as reported in our previous study [28].

In this investigation, the change of wall temperature for every test tube ranges from 50°C (inlet) to 60°C (outlet) and the supersaturation of the test solution remains almost unchanged, so the effect of the wall temperature on scaling can be considered the same for each experiment. Additionally, due to the low flow rate in the test tube (20 L/h or 0.19 m/s) and the low Reynolds number (1800, under laminar flow conditions), the influence of flow rate on scaling might be ignored actually [28].

3. Results and discussion

3.1. Results of orthogonal experiment for HPMA-AEO-9

A standard orthogonal array L_9 (3^4) is used to detect reaction conditions such as the ratio of MA to MA-AEO-9, reaction temperature, the ratio of hydrogen peroxide to monomer, and reaction time [29]. The dose of catalyst ammonium ferric sulfate is only related to the amount of hydrogen peroxide, so the catalyst is not included as an independent factor in the orthogonal test. Table 2 shows the influence of the four independent factors on the scale inhibition performance of HPMA-AEO-9 against calcium carbonate scale. Effects of four factors on the performance of the polymer decrease with the order followed: the ratio of MA to MA-AEO-9, the temperature, the ratio of hydrogen peroxide to the monomer, and the reaction time. The optimum parameter level is $A_2B_3C_2D_1$ and the corresponding optimal conditions are: the molar ratio of MA to MA-AEO-9 is strictly controlled at 6:1; the dose of initiator and catalyst are 7.5 mol% and 0.04 mol% of total monomer, respectively; and the reaction temperature is 95°C.

3.2. Characterization of the synthesized HPMA-AEO-9

3.2.1. Molecular weight determination

Fig. 1 shows the GPC curve of HPMA-AEO-9 (with water as solvent) and the analysis results are listed in Table 3. As shown in Fig. 1, the curve exhibits a single peak and the molecular weight distribution (M_w/M_n) is 2.487. The molecular weight (M_n) of HPMA-AEO-9 is 1299 g/mol which is bigger than that of polymaleic anhydride (HPMA, 625 g/mol) synthesized by Shen et al. [14] and maleic acid based scale inhibitors (<1000 g/mol) reported by Senthilmurugan et al. [30].

3.2.2. FT-IR spectroscopy

The FT-IR spectra of AEO-9, MA-AEO-9, HPMA-AEO-9 and HPMA are presented in Fig. 2. For fatty alcohol polyoxyethylene ether (AEO-9) in (a), the intramolecular H-bonds and single bridge (–OH) stretching are signed at 3411 cm^{-1}. The strong intensity absorption peaks at 2923–2856 cm^{-1} are due to the (–CH_2–) symmetric stretching. The absorption bands at 1462 and 1351 cm^{-1} can be attributed

Table 2
The orthogonal array design (OAD) of HPMA-AEO-9 and corresponding results for calcium carbonate scale inhibition

Number	MA/MA-AEO-9 ratio	Reaction temperature (°C)	H_2O_2 mol%	Reaction time (h)	Inhibition efficiency (%)
1	A_1(5:1)	B_1(85)	C_1(7)	D_1(2)	74.29
2	A_1(5:1)	B_2(90)	C_2(7.5)	D_2(2.5)	81.25
3	A_1(5:1)	B_3(95)	C_3(8)	D_3(3)	78.32
4	A_2(6:1)	B_1(85)	C_3(8)	D_3(3)	92.12
5	A_2(6:1)	B_2(90)	C_2(7.5)	D_1(2)	96.56
6	A_2(6:1)	B_3(95)	C_1(7)	D_2(2.5)	94.35
7	A_3(7:1)	B_1(85)	C_3(8)	D_2(2.5)	78.24
8	A_3(7:1)	B_2(90)	C_1(7)	D_3(3)	80.06
9	A_3(7:1)	B_3(95)	C_2(7.5)	D_1(2)	85.76
K_1	77.95	81.55	82.9	85.54	
K_2	94.34	85.96	87.12	84.61	
K_3	81.35	86.14	82.89	83.5	
R	16.39	4.59	4.23	2.04	

K is the average of every factor scale inhibition rate on calcium carbonate, %; R is the range; and the dosage is 8 mg/L. Scale inhibition rate on calcium carbonate (%) are measured by static scale inhibition method.

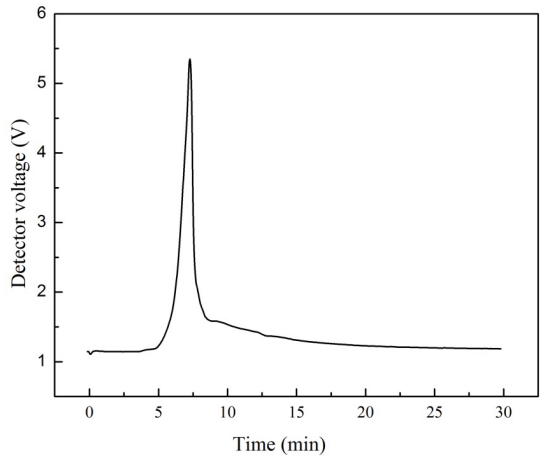

Fig. 1. The molecular weight distribution of HPMA-AEO-9.

Table 3
GPC analysis results of HPMA-AEO-9

Parameter	M_n	M_w	PDI (M_w/M_n)
HPMA-AEO-9	1299	3231	2.487

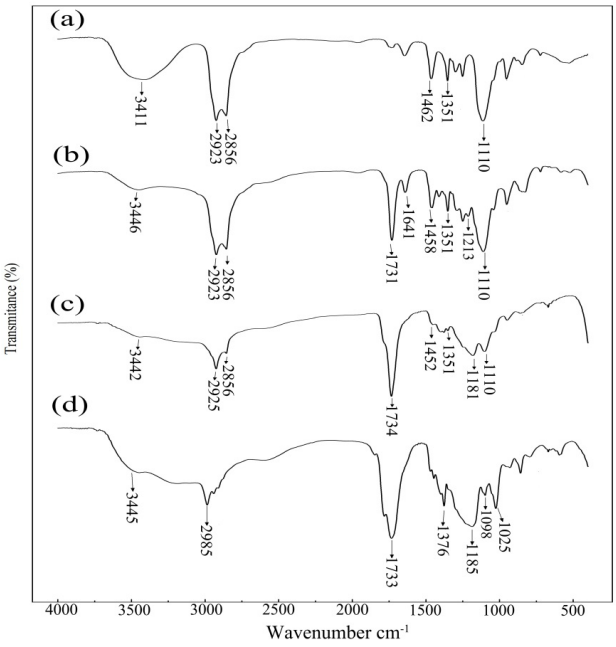

Fig. 2. The FT-IR spectra of AEO-9 (a), MA-AEO-9 (b), HPMA-AEO-9 (c), HPMA (d).

to the (C–H) stretching vibration. The strong sharp peak at 1110 cm^{-1} represents the (–OCH_2CH_2–) stretching vibration [20,31].

For MA-AEO-9 in (b), the (–OH) stretching vibration and H-bonded in acid in MA-AEO-9 are shown at 3446 cm^{-1}. The intensity absorption peaks at 2923–2856 cm^{-1} are due to the (–CH_2–) symmetric stretching. The peak at 1110 cm^{-1} can be due to the characteristic peak of (–CH_2CH_2O–) group. The peak at 1731 cm^{-1} is saturated (–C=O) stretching vibration; the peak at 1641 cm^{-1} represents the (–C=C–) stretching vibration. The absorption bands at 1458 and 1351 cm^{-1} can be due to the stretching vibration of (C-H) group in AEO-9. The peak at 1213 cm^{-1} represents the characteristic stretching vibration of ester (–COC–) group. The vibration of ester (–COC–) group at 1213 cm^{-1}, the (–C=C–) stretching vibration at 1641 cm^{-1} and the saturated (–C=O) stretching vibration at 1731 cm^{-1} clear indicate that MA-AEO-9 has been synthesized successfully.

For HPMA-AEO-9 in (c), the vibration of 3442 cm^{-1} broad intensity absorption band represents the (–OH) stretching vibration and H-bonded in acids in MA-AEO-9 and MA. The peaks at 2925–2856 are due to the (–CH_2–) symmetric stretching, and the peak at 1110 cm^{-1} represents the characteristic peak of (–CH_2CH_2O–) group. The peak at 1734 cm^{-1} is due to saturated (–C=O) stretching vibration in MA-AEO-9 and MA. The peak at 1458 and 1351 cm^{-1} presents the (–CH–) asymmetric stretching vibration in MA-AEO-9 and MA. The peak at 1181 cm^{-1} represents the characteristic stretching vibration of ester (–COC–) group. The (–C=C–) stretching vibration at 1641 cm^{-1} in (b) disappears completely in (c), which reveals that free radical polymerization between MA and MA-AEO-9 has happened.

For the commercial grade HPMA in (d), the vibration of 3445 cm^{-1} broad intensity absorption band is due to H-bonded and the (–OH) stretching vibration. The peak at 1733 cm^{-1} is saturated (–C=O) stretching vibration, The peaks at 2985, 1376 and 1025 cm^{-1} are ascribed to the (–CH–) stretching vibration in MA, the bands at 1185 cm^{-1} can be attributed to the (–COC–) stretching in the acid anhydride [14].

3.2.3. ^1H NMR spectra

HPMA (C_3D_6O, δ ppm): 2.05 (solvent residual peak of C_3D_6O), 2.62–2.84 (–CHC=O, the hydrogen protons on carbon attached to a carbonyl group); 3.18–3.20 (–CHCOC–, protons on carbon attached to anhydride), 4.50–5.17 and 7.20 (–HC=CH–, protons of the olefinic bond), 6.40 (–CHCOOH, protons on carbon connected to carboxyl group) [17]. It is worth noting that the proton peak of the olefin bond still appears at 4.50–5.17 and 7.20 ppm, indicating that a small amount of monomer is still present in the polymer solution.

MA-AEO-9 ($CDCl_3$, δ ppm): 0.83–0.86 (CH_3–, methyl), 1.22 (–CH_2–, methylene), 3.40–3.62 (–CH_2CH_2O–, EO groups) [20]; 4.32–4.34 (–COOCH–, the hydrogen protons on carbon attached to an ester bond); 6.19–6.22 (–CHCOOH, protons on carbon connected to carboxyl group); 6.35–6.37 (–HC=CH–, protons of the olefinic bond); 7.26 (solvent residual peak of $CDCl_3$). All of these reveal that MA-AEO-9 has been synthesized successfully.

HPMA-AEO-9 ($CDCl_3$, δ ppm): 0.85–0.88 (–CH_3, methyl), 1.24–1.27 (–CH_2–, methylene), 2.65–2.76 (–CHC=O, the hydrogen protons on carbon attached to a carbonyl group); 3.43–3.63 (–CH_2CH_2O–, EO groups); 4.13–4.23 (–COOCH–, the hydrogen protons on carbon attached to an ester bond); 6.25 (–CHCOOH, proton of the carbon attached to the carboxyl group); 7.26 (solvent residual peak of $CDCl_3$). It is notable that proton of the olefinic bond at 6.35–6.37

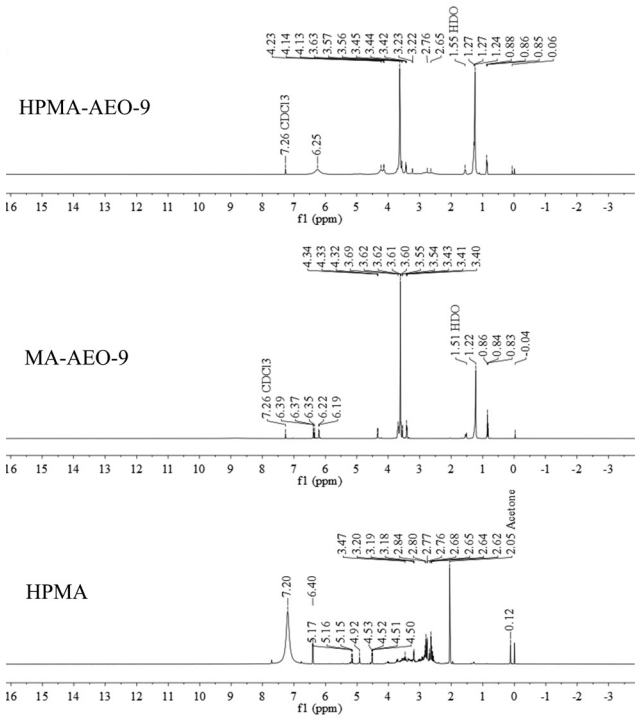

Fig. 3. ^{1}H NMR spectra of HPMA, MA-AEO-9, and HPMA-AEO-9.

ppm disappears, revealing that free radical polymerization among MA and MA-AEO-9 has happened.

Based on the results obtained by FT-IR and ^{1}H NMR, it can be confirmed that the target copolymer HPMA-AEO-9 is obtained in the experiment. According to the integrated area of peaks at 6.25 (–CHCOOH, protons on carbon connected to carboxyl group) and at 3.43–3.63 (–CH_2CH_2O–, EO groups), the number of carboxyl and EO groups in HPMA-AEO-9 molecular are 13 and 9, respectively. Considering the average molecular weight is 1299 g/mol for HPMA-AEO-9 as shown in Fig. 2, so it can be deduced that HPMA-AEO-9 molecular is composed of a polymer backbone (containing six MA units and a MA-AEO-9 unit) and two functional groups like AEO-9 and carboxyl, but the polymer backbone of HPMA includes five MA units.

3.3. Influence of dosage of HPMA-AEO-9 on the inhibition efficiency against $CaCO_3$ scale

Fig. 4 presents the effect of dosage of inhibitor on the inhibition efficiency against $CaCO_3$ scale. As seen from the figure that percent inhibition value (%I) increases steadily from 91% to 100% with dosing of HPMA-AEO-9 from 1 to 5 mg/L and then it decreases slightly with further increase in dosing, which indicates that HPMA-AEO-9 is a threshold inhibitor. However, for the same dosage, %I values of inhibitors show a decline trend with the order followed HPMA-AEO-9 > PAA > HEDP > HPMA, suggesting that the introduction of AEO-9 group into HPMA can significantly improve the inhibitory activity of HPMA-AEO-9 against $CaCO_3$ scale. Specifically, as the typical concentration of scale inhibitor is 4 mg/L, %I value is 99% for HPMA-

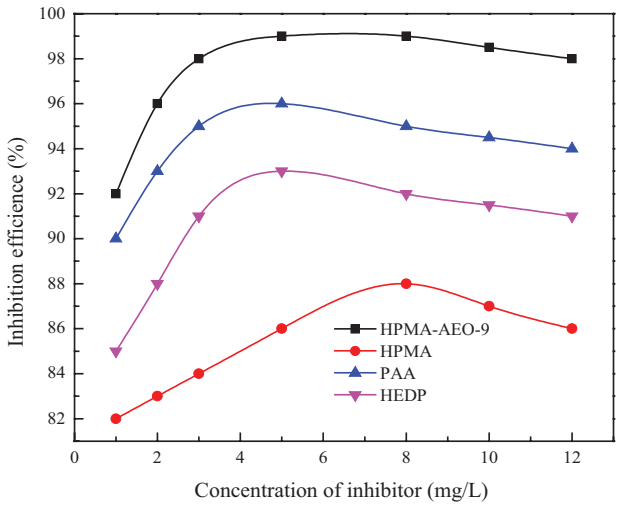

Fig. 4. The effect of dosage of inhibitors on the inhibition efficiency against $CaCO_3$ scale.

AEO-9, 95% for PAA, 92% for HEDP, and 85% for HPMA, revealing that HPMA-AEO-9 used as $CaCO_3$ scale inhibitor are much better than commercial inhibitors like HPMA, PAA and HEDP.

The superior performance of HPMA-AEO-9 over commercial inhibitors may be due to its distinctive polymer structure and scale inhibition mechanism [30,32]. HPMA-AEO-9 has a distinctive polymer structure with its backbone (as HPMA) connected by more carboxylic groups and a soft AEO-9 group (but for HPMA only carboxylic groups). Carboxylic group and AEO-9 group in the molecule of HPMA-AEO-9 can play a synergistic role in dispersing $CaCO_3$ crystal. On the other hand, polycarboxylic acid (PAA, 3000 g/mol), being as a polyelectrolyte threshold inhibitor, contains average 41 acrylic acid units on its polymer backbone as listed in Table 4. The density of carboxyl groups in the molecule of PAA is greater than that of HPMA-AEO-9. The effect of PAA on $CaCO_3$ scale should be much greater than that of HPMA-AEO-9, but this is inconsistent with the experimental results shown in Fig. 4. The main reason for this phenomenon is the presence of EO groups in HPMA-AEO-9. Furthermore, HEDP prevents calcium carbonate scale by sequestering calcium and inhibiting scale precipitation even under conditions of calcite oversaturation [14], but HPMA-AEO-9 inhibiting $CaCO_3$ scale mainly relies on adsorption of carboxyl groups on the crystal surface and weak interaction between EO groups and Ca^{2+}. Thus, the improved performance of HPMA-AEO-9 over HEDP might be due to non-ionic group (AEO-9).

3.4. Influence of Ca^{2+} concentration on the inhibition efficiency against $CaCO_3$ scale

The test conditions are: the concentration of test solution ($\rho(Ca^{2+}) = \rho(HCO_3^-)$) ranges from 250 to 1000 mg/L (as $CaCO_3$), the dosing of inhibitor is 8 mg/L for all the test solutions, and the test solutions are kept at 80°C for 10 h in water bath. Fig. 5 illustrates the effect of Ca^{2+} concentration on the percent inhibition value (%I) for $CaCO_3$ scale in the

Table 4
Density of carboxylate group in polymer molecular

Parameter	Average number of carboxyl	Carboxyl density (wt%)
PAA	41	62
HPMA	8	73
HPMA-AEO-9	13	45

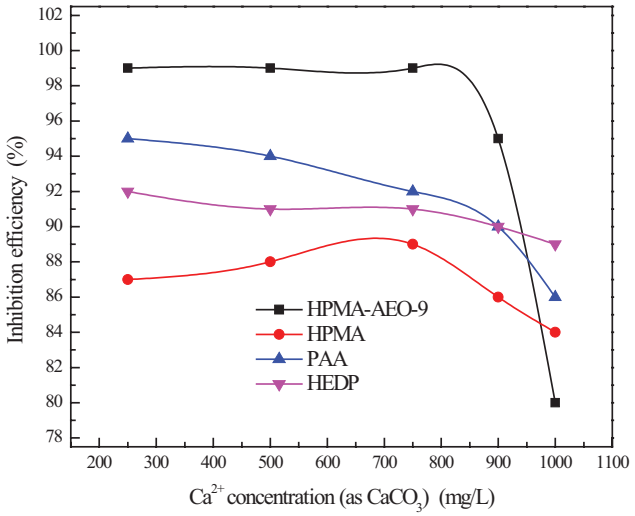

Fig. 5. The effect of Ca^{2+} concentration on the inhibition efficiency against $CaCO_3$ scale.

presence of different scale inhibitors. The anti-scaling efficiency of HPMA-AEO-9 keeps at 99% when Ca^{2+} concentration is less than 750 mg/L and then it decreases quickly from 99% to 84% with Ca^{2+} concentration ranging 750–1000 mg/L. When the calcium concentration is less than 750 mg/L, the Ca^{2+} tolerance of HPMA-AEO-9 has not reached the maximum, and the AEO-9 group to reduce the effective supersaturation would limit a small amount of calcium ions in the solution. However, as Ca^{2+} concentration is 750 mg/L, the Ca^{2+} tolerance of HPMA-AEO-9 has reached its maximum. While the Ca^{2+} concentration exceeds 900 mg/L, a significant decrease in %I is observed in Fig. 5, in this case excess Ca^{2+} in the bulk solution can play a salt bridge effect which may make $CaCO_3$-HPMA-AEO-9 more compact and stable and eventually lead to aggregation and precipitation [30]. On the other hand, for the same Ca^{2+} concentration, %I value decreases with the order followed HPMA-AEO-9 > PAA > HEDP > HPMA as Ca^{2+} concentration is less than 900 mg/L. In summary, HPMA-AEO-9 is good at tolerating calcium compared with other inhibitors as Ca^{2+} concentration is less than 900 mg/L.

3.5. Influence of temperature on the inhibition efficiency against $CaCO_3$ scale

Elevated temperature will increase the saturability (SI) of the calcium carbonate solution and accelerate the formation of calcium carbonate precipitation [32,33]. In this study,

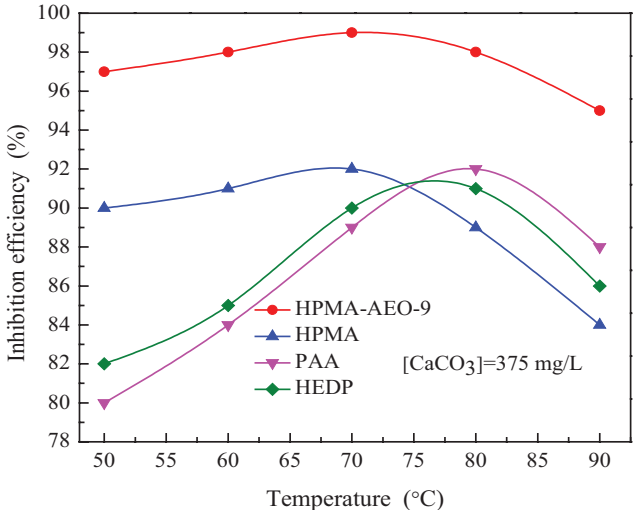

Fig. 6. The effect of temperature on the inhibition efficiency against $CaCO_3$ scale.

a series of static jar tests are conducted with identical conditions as following: both Ca^{2+} and HCO_3^- are 375 mg L^{-1} (as $CaCO_3$), the dosage of scale inhibitors is 8 mg/L, and the specimens are kept reaction at temperature such as 50, 60, 70, 80 and 90°C for 10 h in water bath, respectively. Fig. 6 shows the effect of temperature on the performance of the polymer against $CaCO_3$ scale. %I value of HPMA-AEO-9 increases slowly from 97% to 99% as the temperature ranges from 50 to 70°C, and then it reduces from 99% to 95% with temperature rising from 70 to 90°C. The increase in %I value is owing to the increase of chemical adsorption between calcite crystal and carboxylic ion of HPMA-AEO-9 as well as the decrease in interaction of hydrogen bonds with the elevated temperature [34]. However, the reduction in %I value with elevated temperature may mainly be attributed to formation of micelles with non-ionic (AEO-9) chains of HPMA-AEO-9 in bulk solution [35]. It can also be seen from Fig. 6 that %I value of HPMA-AEO-9 varying with temperature presents a similar tendency as that of HPMA, but it is distinct from PAA and HEDP. Particularly, as the temperature is higher than 80°C, %I value decreases with the order followed HPMA-AEO-9 > PAA > HEDP > HPMA. In the temperature range of 50–90°C, HPMA-AEO-9 has a %I value change of 3%, HPMA of 7%, PAA of 11%, and HEDP of 8%, implying that HPMA-AEO-9 has good thermal stability and temperature has lower impact on HPMA-AEO-9 performance than HPMA, PAA and HEDP. The maximum %I value corresponds to the optimum use temperature of the scale inhibitor, which depends mainly on the scale inhibitor: it is 68°C for HPMA, 80°C for PAA and HEDP, but a temperature ranging 50–80°C for HPMA-AEO-9. With temperature increasing from 50 to 90°C, HPMA-AEO-9 has better inhibition performance than commercial inhibitors obviously, owing to the existence of non-ionic group (AEO-9) in HPMA-AEO-9 molecular. Non-ionic group (AEO-9) can enhance the solubility of HPMA-AEO-9 molecular and make more carboxylic groups exposed in water instead of embedded in the core, which is prone to the adsorption between carboxylic ion of HPMA-AEO-9 and $CaCO_3$ crystal [36]. On the other hand, non-ionic group (AEO-9) can

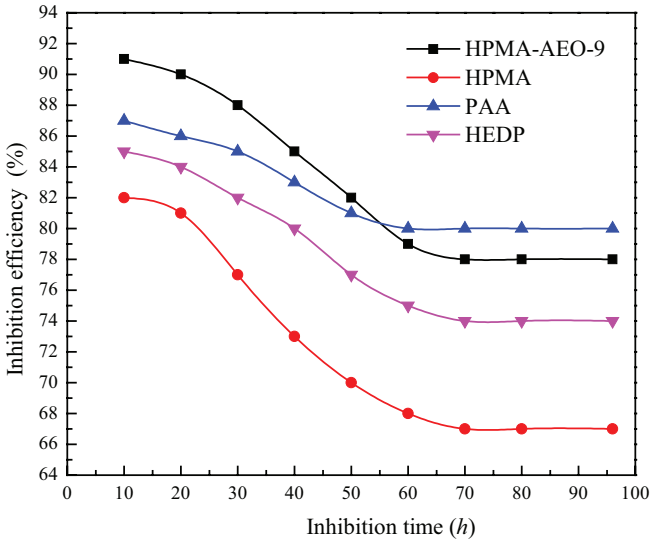

Fig. 7. The effect of heating time on inhibition efficiency against $CaCO_3$ scale.

weaken the interaction between Ca^{2+} and water molecular, causing more Ca^{2+} restricted by EO groups instead of water molecular and thereby reducing SI of $CaCO_3$ solution [34].

3.6. Influence of inhibition time on $CaCO_3$ inhibition

The experimental solutions are composed of 250 mg/L Ca^{2+} (as $CaCO_3$) and 250 mg/L HCO_3^- (as $CaCO_3$) as well as scale inhibitor of 1 mg/L, and the water bath temperature is 80°C. A series of static jar tests are carried out at different scale inhibition time such as 10, 20, 30, 40, 50, 60, 70, 80 and 96 h, respectively. Fig. 7 shows the influence of inhibition time on the scale inhibition efficiency. With the increase of inhibition time, the scale inhibition efficiency of each inhibitor shows a downward trend, and this trend can be divided into three stages: the nucleation-related induction region, the rapid reduction region associated with rapid growth of calcium carbonate scale, and the stable region associated with stable growth of calcium carbonate scale [28]. In inhibition time ranging 10–20 h, %I value decreases slowly with increasing inhibition time, this is due to formation of nucleation on the wall of the jar and in bulk solution simultaneously. The deposition of the stable nuclei on the wall of the jar may lead to Ca^{2+} concentration decline in bulk solution and a slow decrease in %I value. However, in inhibition time ranging 20–70 h, %I value reduces quickly with an increase of inhibition time, which is owing to two facts: the first is that part of HPMA-AEO-9 gradually degrades with inhibition time, resulting in poor adsorption and decline in the inhibition performance [29]; the second is nuclear accumulation and crystal growth with increasing inhibition time [37]. While in the inhibition time of 70–96 h, the Ca^{2+} concentration in bulk solution is very low and the scaling tendency is significantly lowered, thus the decrease in %I value with increasing inhibition time is not significant. Additionally, in the inhibition time ranging 20–96 h, the change of %I value with inhibition time is 7% for PAA, 11% for HEDP, 13% for HPMA-AEO-9, and 15% for HPMA. It is clear that the inhibition time has less effect on the inhibition performance of HPMA-AEO-9 than HPMA, which is due to carboxylic and AEO-9 groups of HPMA-AEO-9 can play a cooperation role in dispersing $CaCO_3$ crystal.

3.7. Influence of pH on the inhibition efficiency against $CaCO_3$ scale

The experimental solutions are composed of 250 mg/L Ca^{2+} (as $CaCO_3$) and 250 mg/L HCO_3^- (as $CaCO_3$) as well as scale inhibitor of 8 mg/L, pH value is adjusted with borax (such as 7.4, 8.0, 8.4, 8.6 and 9.0, respectively), and then the solutions are kept at 80°C for 10 h in water bath. Fig. 8 shows the effect of pH value on the scale inhibition with different antiscalnts. As pH value is less than 8.4, %I value of HPMA-AEO-9 slowly decreases, which is not owing to hydrolysis of HPMA-AEO-9, but to the increase of SI of $CaCO_3$ solution with increasing pH value [37]. However, when pH value is more than 8.4, an obvious reduction in %I value of HPMA-AEO-9 is observed from Fig. 8 and this reduction is smaller than that of HPMA and HEDP. This is owing to the partial hydrolysis of HPMA-AEO-9 to produce HPMA and AEO-9, causing poor adsorption quantity and chelating ability. Additionally for the same pH value, %I value reduces with the order followed HPMA-AEO-9 > PAA > HEDP > HPMA. This is attributed to the fact that the lone pair electrons in the ether bond oxygen atom of HPMA-AEO-9 can form a coordinate bond with the Ca^{2+} ion, so HPMA-AEO-9 is not only highly hydrophilic but also has excellent scale inhibition property [31,34]. Under actual operation conditions, pH is usually controlled in the range of 8.0–8.5, in which %I value significantly changes with different inhibitors: 95–96% for HPMA-AEO-9, 94–95% for PAA, 90–92% for HEDP, and 88–89% for HPMA. Therefore, it is evidence that HPMA-AEO-9 has excellent ability to inhibit calcium carbonate scale at pH ranging 7.4–9.0.

3.8. The effect of concentration of antiscalant on the relative supersaturation of the $CaCO_3$ solution

To evaluate the efficacy of HPMA-AEO-9 as $CaCO_3$ scale inhibitor, a series of conductivity experiments are carried out in the presence of different inhibitors like HPMA-AEO-9, HPMA, PAA and HEDP. Fig. 9 presents the critical supersaturation value (S_r) of $CaCO_3$ solution with the presence of HPMA-AEO-9, HPMA, PAA and HEDP. As seen from Fig. 9, S_r value increases with increasing the dosage of HPMA-AEO-9, and S_r value in the presence of HPMA-AEO-9 is less than that of HPMA for the same dosage. These observations can be explained by two facts. The first is owing to the presence of EO groups in HPMA-AEO-9 molecular, which can reduce conductivity of buck solution through binding Ca^{2+} ions and restricting the mobility of Ca^{2+} ions in water [20]. The second is that HPMA-AEO-9 has a hydrophilic group (AEO-9) which reduces the mobility of HPMA-AEO-9 and leads to a decrease in the conductivity of the bulk solution [17,38]. It also can be seen from Fig. 10 that S_r value of HPMA-AEO-9 increases slowly when the dosage is more than 10 mg/L, which might be due to formation of micelles in bulk solution as mentioned above. Additionally, S_r value of HPMA-AEO-9 is smaller than that of HEDP with dosage ranging 2–12 mg/L, but it is bigger than that of PAA

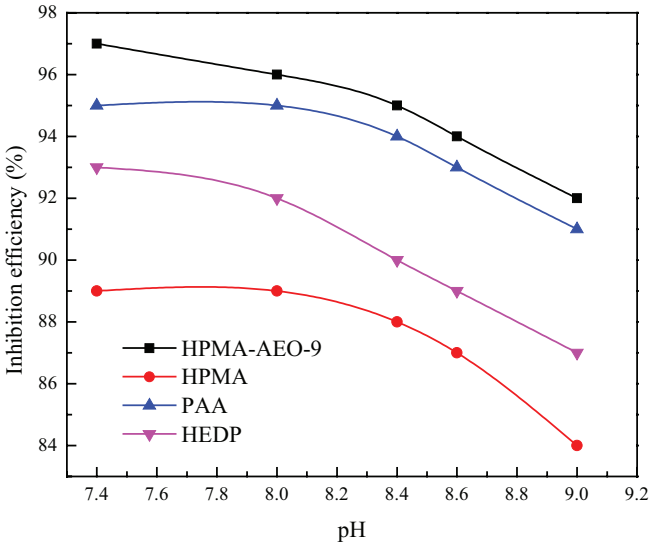

Fig. 8. The effect of pH on the inhibition efficiency against $CaCO_3$ scale.

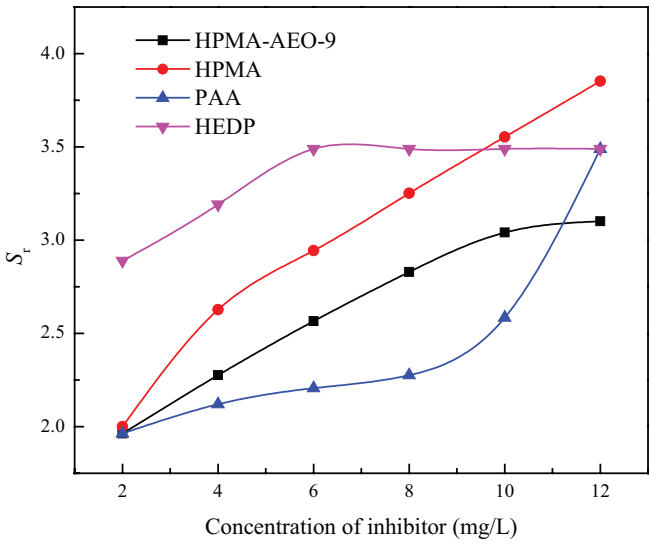

Fig. 9. The effect of dosage of inhibitors on the relative supersaturation of $CaCO_3$ solution.

with dosage being less than 11 mg/L. In general, the impact of HPMA-AEO-9 on S_r of $CaCO_3$ solution is less than that of HPMA.

3.9. The effect of run time on the mean growth rate of scaling

To investigate the influence of scale inhibitor on the growth process of $CaCO_3$ scale, dynamic tests have been carried out with the presence of HPMA-AEO-9 and HPMA, respectively. It is noted that for each inhibitor, the test is repeated at least three times and the test results are presented in Fig. 10. As shown in the figure, the growth process of $CaCO_3$ scale can be divided into three stages: the

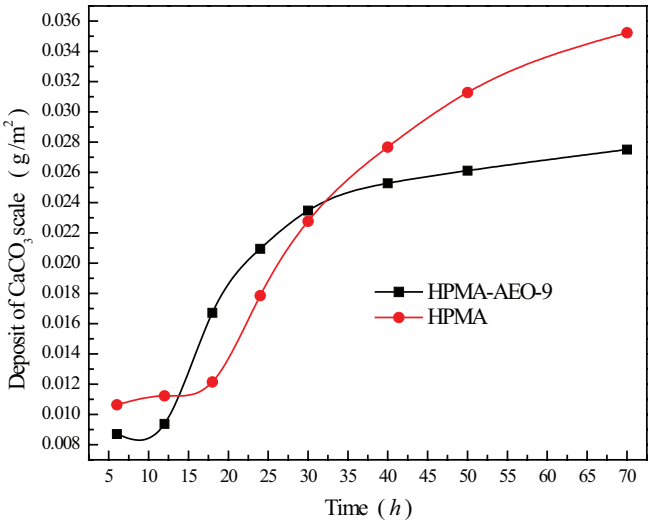

Fig. 10. The effect of run time on deposit of $CaCO_3$ scale.

induction region where the scale growth is independent upon run time practically, the rapid growth region where the scale growth increases rapidly with run time, and the stable growth region where the scale growth presents an asymptotic trend. Each region can be matched with different development phases in the scaling process: nucleation phase, rapid growth phase and asymptotic/falling phase [39]. The scale growth actually relies on the performance of inhibitor to interfere with two steps such as nucleation and crystal growth [40].

In the induction region, the induction region is longer than 18 h for HPMA and shorter than 12 h for HPMA-AEO-9 as illustrated in Fig. 10. Figs. 11a and b illustrate SEM pictures of $CaCO_3$ scaling on the tube wall after 12 h. It can be observed from the figures that the additive of HPMA-AEO-9 can obviously inhibit the nucleation rate (reflected by the particle number and the crystallite sizes). Therefore, the growth rate of the scale in the presence of HPMA-AEO-9 is lower than that of HPMA as shown in Fig. 10. The strong inhibition of nucleation by HPMA-AEO-9 can mainly be ascribed to three facts. The first is AEO-9 group could bind Ca^{2+} ion (weak interaction) and thus reduce SI of $CaCO_3$ solution [41]. The second is adsorption of HPMA-AEO-9 as a surfactant on the tube wall causing surface free energy decline, which is not conducive to the formation of stable nuclei on the tube wall [32]. The third is HPMA-AEO-9 as a threshold inhibitor that can affect the initial clustering process of the proto nuclear.

In the rapid growth region, the scale growth usually occurs on many stable nucleuses formed in the induction region on the tube wall. Figs. 11c and d indicate SEM pictures of $CaCO_3$ scaling on the tube wall after 24 h. The particle number with additive of HPMA-AEO-9 is less than that of HPMA and especially the number of small nuclei in Fig. 11d is much more than that in Fig. 11c, but the average particle sizes with presence of HPMA-AEO-9 is bigger than that of HPMA. It is clear that neo-nucleation activity is significantly inhibited by HPMA-AEO-9 even in the rapid growth region. It can also be seen from Fig. 10 that the growth rate in the presence of HPMA-AEO-9 is higher than that of HPMA at

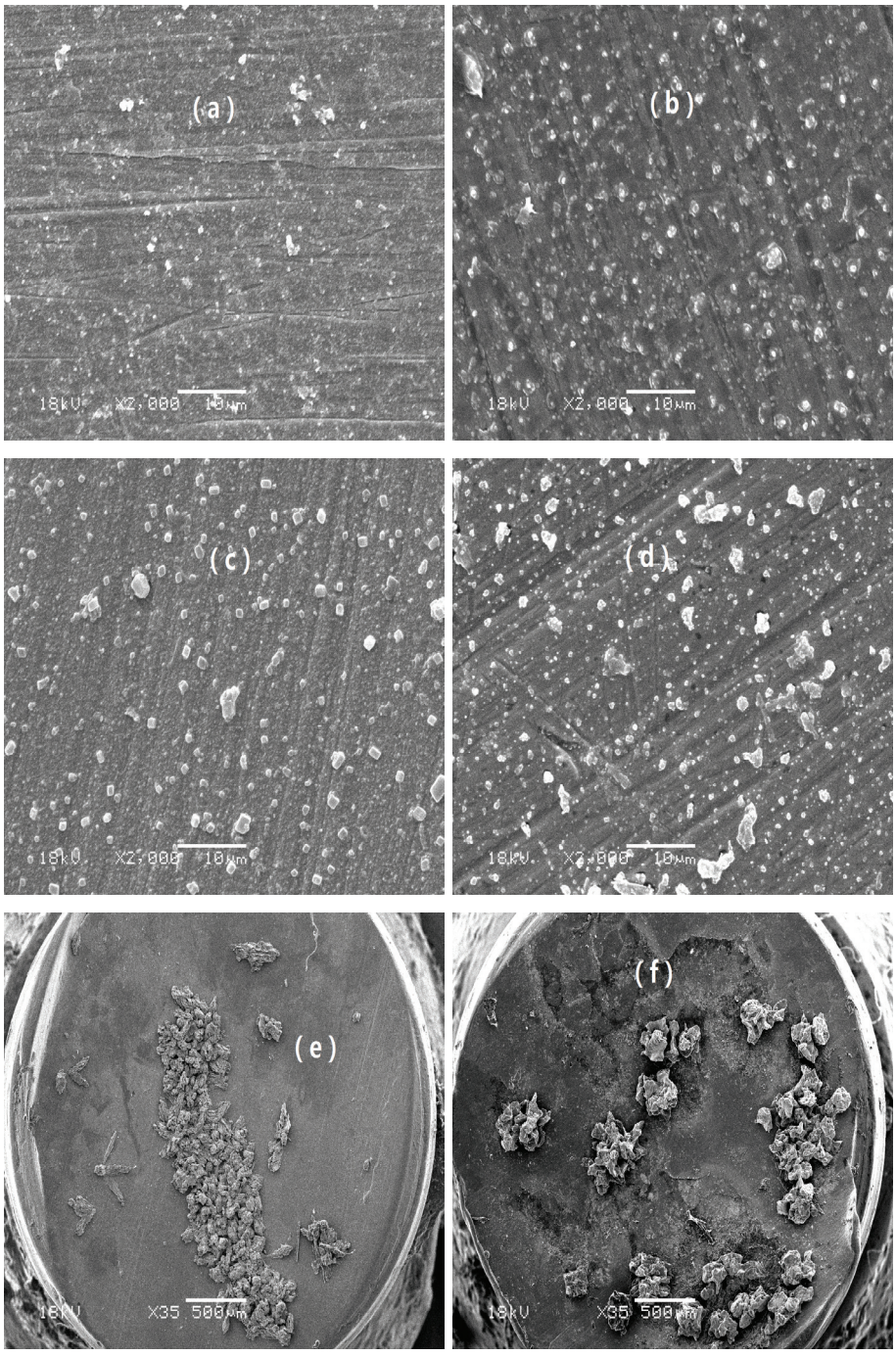

Fig. 11. SEM pictures of $CaCO_3$ with HPMA-AEO-9 in 12 h (a), $CaCO_3$ with HPMA in 12 h (b), $CaCO_3$ with HPMA-AEO-9 in 24 h (c), $CaCO_3$ with HPMA in 24 h (d), $CaCO_3$ with HPMA-AEO-9 in 70 h (e), $CaCO_3$ with HPMA in 70 h (f).

the same run time. This is attributed to the large formation of crystal nuclei on the test tube wall in the presence of HPMA, which prevents heat transfer and reduces the temperature as well as the concentration of calcium carbonate near the test tube wall, thereby reducing the scaling rate [28].

In the stable growth region, Figs. 11e and f illustrate SEM pictures of $CaCO_3$ scaling on the tube wall during run time of 70 h. The particle sizes with presence of HPMA-AEO-9 and HPMA ranges from 100 to 500 μm, but for HPMA-AEO-9 particles with a diameter under 100 μm account for the majority, while for HPMA particles being larger than 200 μm in diameter dominate. Additionally, the growth rate with the additive of HPMA-AEO-9 is lower than that of HPMA at the same run time as shown in Fig. 10, due to the effect of HPMA-AEO-9 on $CaCO_3$ scaling being more than that of HPMA as mentioned above.

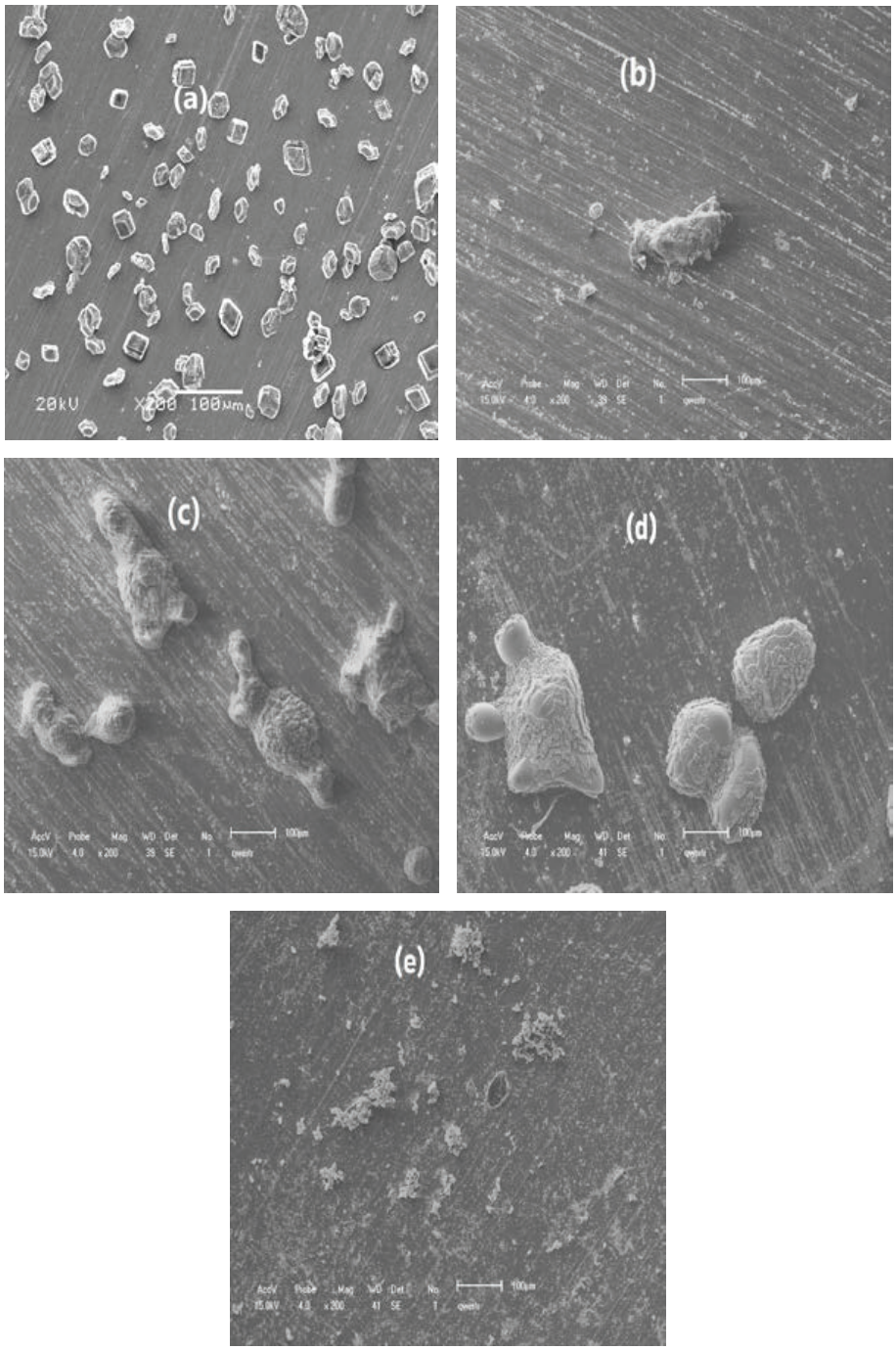

Fig. 12. SEM pictures of $CaCO_3$ with absence of inhibitor (a), HPMA-AEO-9 (b), with HPMA (c), with PAA (d), with HEDP (e).

3.10. The impact of HPMA-AEO-9 on SEM and XRD of $CaCO_3$ crystals

The experimental conditions for preparing $CaCO_3$ crystal samples are the same as showed in Section 3.3 and 3.4, but the water samples are composed of 600 mg/L Ca^{2+} (as $CaCO_3$) and 600 mg/LCO_3^{2-} (as $CaCO_3$) as well as 8 mg/L of scale inhibitor. The deposit of calcium carbonate scale on the cylinder (ø3×4 mm) [27] is studied using scanning electron microscope (SEM). Calcium carbonate precipitation is filtered, washed, dried and finally analyzed using X-Ray Diffraction (XRD). Fig. 12 illustrates the SEM pictures of $CaCO_3$ scale with the presence of HPMA-AEO-9, HPAM, PAA and HEDP, respectively. Fig. 13 shows the XRD of calcium carbonate precipitation in the presence and absence of inhibitors.

Fig. 12a shows the calcium carbonate crystals without inhibitors on the test tube wall, most of them are diamond-shaped calcite with regular shape and smooth surface. These agree with XRD analysis in Fig. 13a that the crystal

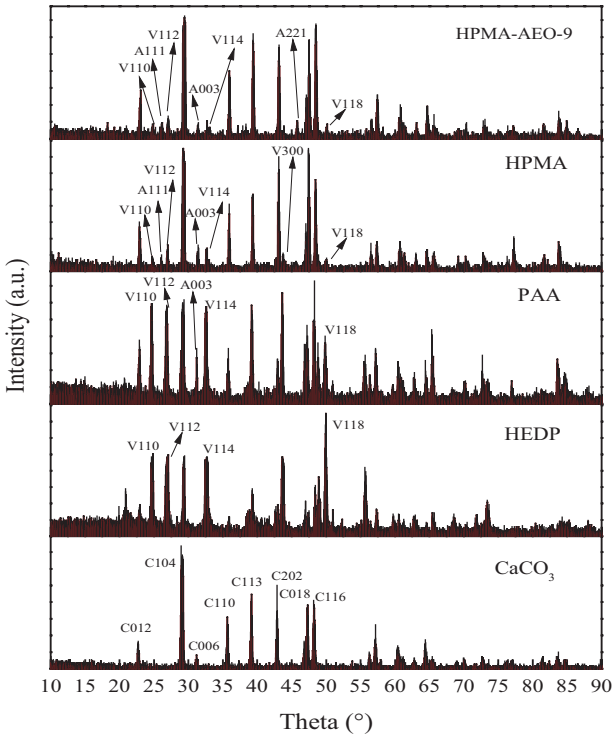

Fig. 13. XRD analysis of $CaCO_3$ crystals with the absence of inhibitor (a), with HEDP (b), with PAA (c), with HPMA(d), with HPMA-AEO-9(e).

type is all calcite which is proved by the diffraction peaks at C(104), C(012), C(113) and C(202). In the presence of HPMA-AEO-9, a small and loose $CaCO_3$ deposit is observed in Fig. 12b, which is attributed to the synergistic effect of the two functional groups (–COOH and AEO-9) of HPMA-AEO-9 on the crystal nucleus. But in the presence of HPMA or PAA, calcium carbonate crystals exhibit a large spherical pseudo-spherical shape in Figs. 12c and d, which is formed by the interaction between HPMA or PAA and the surface of the crystal nucleus [42,43]. While in the presence of HEDP, more snowflake-like $CaCO_3$ crystals are scattered on the metal wall and their size is less than 20 μm in Fig. 12e.

It can be seen from Figs. 12 and 13 that in the presence of scale inhibitors the calcium carbonate crystal is significantly changed. The diffraction peaks at C(104), C(012), C(113) and C(202) can be assigned to the characteristic peaks of calcite; but the peaks at A(111), A(003) and A(221) are for aragonite; while the peaks at V(004), V(110), V(112), V(114), V(300) and V(118) are for vaterite [44,45]. The $CaCO_3$ precipitates in the absence of inhibitor are consisted of 100% calcite; but in presence of HPMA, approximately 86% calcite, 11% vaterite, and 3% aragonite; while in presence of HPMA-AEO-9, approximately 82% calcite, 12% vaterite, and 6% aragonite. It is obvious that HPMA-AEO-9 can effectively inhibit the formation of crystal nucleus and change calcium carbonate crystal from stable calcite to unstable aragonite and vaterite, making the calcium carbonate deposits soft and loose and easily being washed away by water.

The inhibition performance of HPMA-AEO-9 against calcium carbonate scale is mainly due to interactions between $CaCO_3$ crystal and carboxylic ion as well as EO

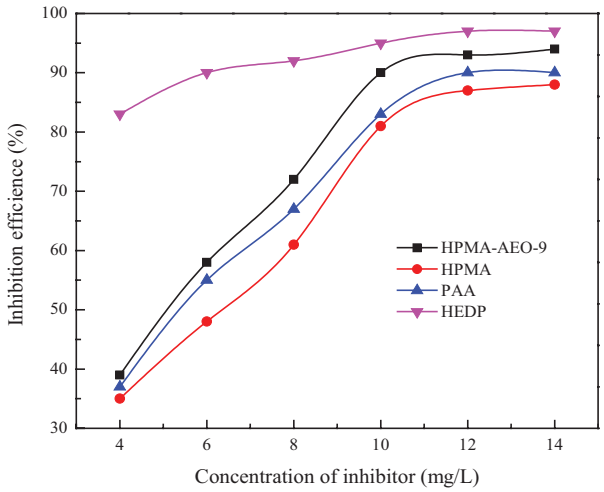

Fig. 14. The effect of dosage of inhibitors on scaling of Yellow River water.

groups and Ca^{2+} ion. AEO-9 group can bind Ca^{2+} ions (weak interaction) and form complexes with the excellent solubility, thereby reducing the effective supersaturation during precipitation [36,46]. AEO-9 group can also exhibit great dispersion stability due to its high electrostatic interaction, which reduces the electrostatic repulsion between the polar heads (carboxylic acid groups) of HPMA-AEO-9 and lower down the surface energy of HPMA-AEO-9 micelles, leading to an increase in the aggregation number of HPMA-AEO-9 molecules and enlarging HPMA-AEO-9 micelles [32,34,36,46]. When HPMA-AEO-9 adsorbs on the surface of calcium carbonate crystal, the presence of dodecyl in the AEO-9 group will greatly affect the growth of calcium carbonate crystals and this effect will be far greater than those caused by HPMA molecule.

3.11. Application of HPMA-AEO-9 in concentrated water of Yellow River

The composition of the concentrated water of Yellow River is: 730 mg/L Ca^{2+}, 55 mg/L Mg^{2+}, 140 mg/L HCO_3^-, 20 mg/L CO_3^{2-}, 270 mg/L Cl^-, 600 mg/L SO_4^{2-}, 15 mg/L SiO_2, 5 mg/L PO_4^{3-}, pH value is 8.4 and the concentration ratio is 5. The pH of test solutions is strictly adjusted with borax to give a pH value of 8.4. The test samples are heated in water bath at 60°C for 10 h, then cooled to room temperature, and finally determined by EDTA titration. As reported in our previous research that under the conditions mixed-scale is mainly composed of calcium carbonate, in addition to a small amount of calcium sulfate and calcium phosphate and calcium silicate as well as magnesium hydroxide [39]. Fig. 14 shows the variation of inhibition efficiency against mixed-scale with the dosage of scale inhibitors. As seen from Fig. 14 that the scale inhibition efficiency increases with the dosage from 4 mg/L to 10 mg/L, and then it remained same when the dosage is over 10 mg/L. The highest efficiency is 96% for HEDP, 91% for HPMA-AEO-9, 88% for PAA and 85% for HPMA. However, for the same dosing of inhibitor, the inhibition efficiency decreases with the order followed HEDP > HPMA-AEO-9 > PAA > HPMA,

which is mainly because HEDP can inhibit the formation of mixed-scale with the presence of interaction of phosphono and hydroxyl [47].

4. Conclusions

HPMA-AEO-9 is prepared from maleic anhydride, AEO-9, ammonium ferric sulfate and hydrogen peroxide by the way of free radical copolymerization. The structure and M_w of the polymer are characterized by FT-IR, ^{1}H NMR and GPC. The main results can be summarized as following:

(a) HPMA-AEO-9 used as $CaCO_3$ scale inhibitor is much better than commercial inhibitors such as HPMA, PAA and HEDP. The presence of AEO-9 group can enhance the solubility of the polymer and improve the performance of the polymer. The impact of pH on the performance of HPMA-AEO-9 is not obvious at the pH ranging 7.4–8.5; the effect of temperature is more pronounced than that of pH; Ca^{2+} concentration has lightly impact on the performance of HPMA-AEO-9 as Ca^{2+} concentration is less than 750 mg/L.
(b) Compared with addictive of HPMA, the presence of HPMA-AEO-9 can obviously inhibit the nucleation rate at the induction region, accelerate the growth of nuclei at the rapid growth region, and low down the growth rate of scaling at the stable growth region.
(c) SEM and XRD analysis show that morphologies of $CaCO_3$ scale are distorted with the presence of HPMA-AEO-9.

Acknowledgments

This work is supported by the National Natural Science Foundation of China (No. 51166007).

References

[1] S. Zhang, H. Qu, Z. Yang, C. Fu, Z. Tian, W. Yang, Scale inhibition performance and mechanism of sulfamic/amino acids modified polyaspartic acid against calcium sulfate, Desalination, 419 (2017) 152–159.
[2] M. Chaussemier, E. Pourmohtasham, D. Gelus, N. Pécoul, H. Perrot, J. Lédion, H.C. Charpentier, O. Horner, State of art of natural inhibitors of calcium carbonate scaling, A review article, Desalination, 356 (2015) 47–55.
[3] Y. Liu, A. Kan, Z. Zhang, C. Yan, F. Yan, F.F. Zhang, N. Bhandari, Z.Y. Dai, G. Ruan, L. Wang, J. Greenberg, M. Tomson, An assay method to determine mineral scale inhibitor efficiency in produced water, J. Petrol. Sci. Eng., 143 (2016) 103–112.
[4] K. Halake, H.J. Kim, M. Birajdar, B.S. Kim, H. Bae, C.C. Lee, Y.J. Kim, S. Kim, S. Ahn, S.Y. An, S.H. Jung, J. Lee, Recently developed applications for natural hydrophilic polymers, J. Ind. Eng. Chem., 40 (2016) 16–22.
[5] D. Hasson, H. Shemer, A. Sher, State of the art of friendly "green" scale control inhibitors: a review article, Ind. Eng. Chem. Res., 50 (2011) 7601–7607.
[6] W. Shi, W. Xu, H. Cang, X.H. Yan, R. Shao, Y.H. Zhang, M.Z. Xia, Design and synthesis of biodegradable antiscalant based on MD simulation of antiscale mechanism: A case of itaconic acid-epoxysuccinate copolymer, Comp. Mater. Sci., 136 (2017) 118–125.
[7] Y. Wang, A. Li, H. Yang, Effects of substitution degree and molecular weight of carboxymethyl starch on its scale inhibition, Desalination, 408 (2017) 60–69.
[8] S.M. Thombre, B.D. Sarwade, Synthesis and biodegradability of polyaspartic acid: a critical review, J. Macromol. Sci., 42 (2005) 1299–1315.
[9] Y.A. Issabayev, G.I. Boiko, N.P. Lyubchenko, Y.M. Shaikhutdinov, HervéMuhr, L. Colombeau, P. Arnoux, C. Frochot, Synthesis of unexplored aminophosphonic acid and evaluation as scale inhibitor for industrial water applications, J. Water Process Eng., 22 (2018) 192–202.
[10] L. Yang, W.Z. Yang, B. Xu, X.S. Yin, Y. Chen, Y. Liu, Y. Jia, Y. Huan, Synthesis and scale inhibition performance of a novel environmental friendly and hydrophilic terpolymer inhibitor, Desalination, 416 (2017) 166–174.
[11] E.G. Darton, Membrane chemical research: centuries apart, Desalination, 132 (2000) 121–131.
[12] A. Zahid, G.K. Petros, Evaluation of maleic acid based polymers as scale inhibitors and dispersants for industrial water applications, Desalination, 335 (2014) 55–63.
[13] A. Martinod, M. Euvrard, A. Foissy, A. Neville, Progressing the understanding of chemical inhibition of mineral scale by green inhibitor, Desalination, 220 (2008) 345–352.
[14] Z.H. Shen, J.S. Li, K. Xu, L.L. Ding, H.Q. Ren, The effect of synthesized hydrolyzed polymaleic anhydride (HPMA) on the crystal of calcium carbonate, Desalination, 284 (2012) 238–244.
[15] F. Yan, F.F. Zhang, B. Narayan, L. Wang, Z.Y. Dai, Z. Zhang, Y. Liu, G.D. Ruan, K. Amy, T. Mason, Adsorption and precipitation of scale inhibitors on shale formations, J. Petrol. Sci. Eng., 13 (2015) 32–40.
[16] D.L. Verraest, J.A. Peters, H. Van Bekkum, G.M. Van Rosmalen, Carboxymethyl inulin: a new inhibitor for calcium carbonate precipitation, J. Am. Oil Chem. Soc., 73 (1996) 55–62.
[17] L. Ling, Y.M. Zhou, J.Y. Huang, Q.Z. Yao, G.Q. Liu, P.X. Zhang, W. Sun, W.D. Wu, Carboxylate –terminated double-hydrophilic block copolymer as an effective and environmental inhibitor in cooling water systems, Desalination, 304 (2012) 33–40.
[18] A. Alhamzah, C.M. Fellows, Apparent inhibition of thermal decomposition of hydrogen carbonate ion by poly(acrylic acid), The effect of molar mass and end-group functionality, Desalination, 332 (2014) 33–43.
[19] H.C. Wang, Y.M. Zhou, Q.Z. Yao, Y.Y. Bu, Y.Y. Chen, W. Sun, Study on calcium scales inhibition performance in the presence of double-hydrophilic copolymer, Int. J. Polym. Mater. Po., 64 (2015) 205–213.
[20] G.Q. Liu, M.W. Xue, H. Yang, Polyether copolymer as an environmentally friendly scale and corrosion inhibitor in seawater, Desalination, 419 (2017) 133–140.
[21] F. Chen, N.A. Kolson, Water soluble copolymers, U.S. Patent: 644474, 2002, 09, 03.
[22] H. Füredi-Milhofer, S. Sarig, Interactions between polyelectrolytes and sparingly soluble salts, Prog. Cryst. Growth Ch., 32 (1996) 45–74.
[23] Q.H. Deng, H.P. Li, H.Y. Sun, Y.G. Sun, Y. Lia, Hyperbranched exopolysaccharide-enhanced foam properties of sodium fatty alcohol polyoxyethylene ether sulfate, Colloids Surf., 141 (2016) 206–212.
[24] H. Zhang, D. Wei, F. Xu, P. Cai, J. Zhang, The latest synthesis process of hydrolyzed polymaleic anhydride, Appl. Chem. Ind., 12 (2008) 1478–1480. (In Chinese)
[25] Y. Xu, B. Zhang, L.L. Zhao, Y.C. Cui, Synthesis of polyaspartic acid/5-aminoorotic acid graft copolymer and evaluation of its scale inhibition and corrosion inhibition performance, Desalination, 311 (2013) 156–161.
[26] L.C. Wang, K. Cui, L.B. Wang, H.X. Li, S.F. Li, Q.L. Zhang, H.B. Liu, The effect of ethylene oxide groups in alkyl ethoxy carboxylates on its scale inhibition performance, Desalination, 379 (2016) 75–84.
[27] A. Jada, R.A. Akbour, C. Jacquemet, J.M. Suau, O. Guerret, Effect of sodium polyacrylate molecular weight on the crystallogenesis of calcium carbonate, J. Cryst. Growth, 306 (2007) 373–382.

[28] L.C. Wang, S.F. Li , L.B. Wang, K. Cui, Q.L. Zhang, H.B. Liu , G. Li, Relationships between the characteristics of $CaCO_3$ fouling and the flow velocity in smooth tube, Exp. Therm. Fluid Sci., 74 (2016) 143–159.
[29] C. Wang, D. Zhu, X. Wang, Low-phosphorus maleic acid and sodium q-styrenesulfonate copolymer as calcium carbonate scale inhibitor, J. Appl. Polym. Sci., 115 (2010) 2149–2155.
[30] B. Senthilmurugan, B. Ghosh, S.S. Kundu, M. Haroun, B. Kameshwari, Maleic acid based scale inhibitors for calcium sulfate scale inhibition in high temperature application, J. Petrol. Sci. Eng., 75 (2010) 189–195.
[31] K. Du, Y.M. Zhou, L.Q. Wang, Y.Y. Wang, Synthesis and properties of environmentally friendly calcium phosphate inhibitor, Tenside Surfact. Det., 6 (2009) 152–158.
[32] X. Yue, X. Fan, Q. Li, X. Chen, C. Wang, Aggregation behaviors of alkyl ether carboxylate surfactants in water, J. Mol. Liq., 227 (2017) 161–167.
[33] Q.W. Wang, F. Liang, W. Al-Nasser, F. Al-Dawood, T. Al-Shafai, H. Al-Badairy, S.W. Shen, H. Al-Ajwad, Laboratory study on efficiency of three calcium carbonate scale inhibitors in the presence of EOR chemicals, Petroleum, 4(4) (2018) 375–384.
[34] Y.J. Chen, G.Y. Xu, Improvement of Ca^{2+}-tolerance by the introduction of EO groups for anionic surfactants: Molecular dynamics simulation, Colloids Surf., 424 (2013) 26–32.
[35] P. Parekh, D. Varade, J. Parikh, P. Bahadur, Anionic-cationic mixed surfactant systems: micellar interaction of sodium dodecyl trioxyethylene sulfate with cationic gemini surfactants, Colloids Surf., 385 (2011) 111–120.
[36] Y.M. Zhang, J.P. Niu, Q.X. Li, Synthesis and properties evaluation of sodium fatty alcohol polyoxyethylene ether sulfonate, Tenside Surfact. Det., 47 (2010) 34–39.
[37] H.L. Golterman, M.L. Meyer, The geochemistry of two hard water rivers, the Rhine and the Rhone. Part 2: The apparent solubility of Calcium carbonate, Hydrobiologia, 126 (1985) 11–19.
[38] A. Martinod, A. Neville, M. Euvrard, K. Sorbie, Electrodeposition of a calcareous layer: Effects of green inhibitors, Chem. Eng. Sci., 64 (2009) 2413–2421.
[39] L.C. Wang, Q.L. Zhang, L. Wang, L.B. Wang, X.J. Wang, X.S. Ju, K. Cui, C.G. Zhu, The performance of a polymaleic-based polymeric scale inhibitor on $CaCO_3$ inhibition under different water quality variables, Desal. Water Treat., 85 (2017) 36–45.
[40] M.G. Mwaba, M.R. Golriz, J. Gu, A semi-empirical correlation for crystallization fouling on heat exchange surfaces, Appl. Therm. Eng., 26 (2006) 440–447.
[41] X.R. Guo, F.X. Qiu, K. Dong, X. Zhou, J. Qi, Y. Zhou, D.Y. Yang, Preparation, characterization and scale performance of scale inhibitor copolymer modification with chitosan, J. Ind. Eng. Chem., 18 (2012) 2177–2183.
[42] A.A. Al-Hamzah, C.M. Fellows, A comparative study of novel scale inhibitors with commercial scale inhibitors used in seawater desalination, Desalination, 359 (2015) 22–25.
[43] K. Song, W. Kim, S. Park, J.H. Bang, C.W. Jeon, J.W. Ahn, Effect of polyacrylic acid on direct aqueous mineral carbonation of flue gas desulfurization gypsum, Chem. Eng. J., 301 (2016) 51–57.
[44] S.I. Kuriyavar, R. Vetrivel, S.G. Hegde, A.V. Ramaswamy, D. Chakrabarty, S. Mahapatra, Insights into the formation of hydroxyl ions in calcium carbonate: temperature dependent FTIR and molecular modelling studies, J. Mater. Chem., 10 (2000) 1835–1840.
[45] Y.M. Tang, W.Z. Yang, X.S.Yin, Y. Liu, P.W. Yin, J.T. Wang, Investigation of $CaCO_3$ scale inhibition by PAA, ATMP and PAPEMP, Desalination, 228 (2008) 55–62.
[46] W. Yan, Z. Chen, Q. Yu, W. Zhu, H. Wang, B. Du, Effects of fatty alcohol polyoxyethylene ether AEO on PbO_2 structure and electrodeposition behavior, J. Electrochem. Soc., 163 (2016) 414–420.
[47] A. Khormali, A.R. Sharifov, D.I. Torba, Increasing efficiency of calcium sulfate scale prevention using a new mixture of phosphonate scale inhibitors during water flooding, J. Petrol. Sci. Eng., 164 (2018) 245–258.